Structural and Superconducting Properties of Magnetically Doped Bi-2212 Textured Rods Grown by Laser Floating Zone (LFZ) Technique

M.E. Yakinci[1], M.A. Madre[2], M. Ozabaci[1], A. Sotelo[2]

[1]SEM/EDX Laboratuvarı, Bilimsel ve Teknolojik Arastırma Merkezi (˙IBTAM), Inönü Üniversitesi, 44280 Malatya, Turkey

[2] Instituto de Ciencia de Materiales de Aragón (ICMA), CSIC-Universidad de Zaragoza, Maria de Luna, 3, 50018 Zaragoza, Spain

Abstract

In this work, we have applied the laser floating zone technique, a well-known method to produce highly aligned crystals and dense morphology, with improved transport properties, to obtain $Bi_2Sr_2CaCu_{2-x}Ni_xO_8$ (x = 0, 0.01, 0.03, 0.05 and 0.1) fibers of about 1.8 mm diameter ×12 cm length. Microstructural and magnetic properties of textured materials grown in the optimum conditions were analyzed through scanning electron microscope (SEM), energy dispersive X-ray analysis (EDX), powder XRD patterns, *M*–*T* and *M*–*H* loops. XRD analysis showed that addition of Ni at x = 0.1 level caused the formation of small amounts of Bi-2201 phase. Thermal treatment has produced the agglomeration of Ni particles up to a few μm, detected by dot mapping EDX. Both T_c-onset and J_{cmag} values of the annealed rods decreased with the increasing Ni substitution rate, determined from the *M*–*T* and *M*–*H* loops, respectively.

Keywords: Bi-2212; Textured material; Floating zone; Magnetic substitution

Corresponding Author: M.E. Yakinci SEM/EDX Laboratuvarı, Bilimsel ve Teknolojik Arastırma Merkezi (IBTAM), Inönü Üniversitesi, 44280 Malatya, Turkey
e-mail: eyyuphan.yakinci@inonu.edu.tr.

1 Introduction

Bi-based superconductors family is formed by three different phases, with a general formula $Bi_2Sr_2Ca_{n-1}Cu_nO_{2n+4}$ where n = 1, 2 and 3. The n = 2 and 3 members have shown great potential to produce power cables and coils, as well as fault current limiters, when they are properly processed [1–3]. Of these two members, n = 2 is the most used for practical applications due to its easier preparation, higher stability, lower sensitivity to oxygen stoichiometry, and relatively high T_c, compared with the n = 3 member. Melt processing techniques, which are based on the principle of recrystallization of partially molten polycrystalline powder to produce the oriented structure, are often used for the production of materials having the desired shape and strong grain connectivity with a high degree of alignment. Among the melt processing techniques used to fabricate textured HT_c superconducting materials, the laser floating zone (LFZ) method has demonstrated to be a very effective way for growing aligned rods with high critical current densities [4–8].

In terms of technological applicability of HT_c superconducting materials, the main limitations have been caused by the weak link effect between superconducting grains and weak pinning of flux lines [9]. Much effort has been devoted so far to overcome these obstacles by producing artificial pinning centers through the addition of dopants or creating defects [10,11]. For this purpose, Pb, Ag, Ti and MgO additions and substitutions have already been performed to the Bi-2212 phase with the LFZ technique [7,12–14]. It has been shown that adding of Ag up to 1 wt.% improved the microstructure and mechanical strength by reducing the porosity [7,12]. Similarly, MgO addition to Bi-2212 flat monoliths realized by a different laser processing method (laser zone melting, LZM) strengthen the critical current density by a factor of 3 without any observable degradation on texturing level [14]. In contrast, addition of 2 at.% Ti degraded both texturing and superconducting parameters of rods by introducing bubbles into the structure which eventually causes a decrease in grain size [13].

Within this scope, the effect of Ni for Cu substitution on the texturing and superconducting properties of LFZ grown rods having a $Bi_2Sr_2CaCu_{2-x}Ni_xO_{8+\delta}$

stoichiometry *(x* = 0*,* 0.01*,* 0.03*,* 0.05*,* 0.1*)* has been investigated in this study. The main goal of this study is increasing the critical current density by enhancing flux pinning properties together with a higher density and better grain alignment in the rods.

2 Experimental

$Bi_2Sr_2CaCu_{2-x}Ni_xO_{8+\delta}$ (x = 0, 0.01, 0.03, 0.05, 0.1) polycrystalline samples were synthesized using the classical solid state method. Commercial Bi_2O_3 (Panreac, 98+%), $SrCO_3$ (Panreac, 98+%), $CaCO_3$ (Panreac, 98.5+%), CuO (Panreac, 97+%) and NiO (Aldrich, %99) powders were weighed in the adequate atomic proportions and ball-milled using agate balls and acetone for 30 min at 300 rpm to obtain a homogeneous mixture. The resulting suspension was dried using an IR evaporation system in order to vaporize the maximum amount of acetone. The resulting mixture was placed in a furnace and heated slowly to 750 °C, where it was kept for ca. 12 h, followed by furnace cooling. After cooling, the remaining powder was manually ground and heated again at 800 °C for 12 h, milled and isostatically pressed at ca. 200 MPa in form of cylinders (1.5–3 mm diameter and 120 mm long).

The obtained cylinders were subsequently used as feed in a directional solidification process performed in a LFZ installation described elsewhere in detail [15]. The textured bars were obtained using a continuous power Nd:YAG laser (λ = 1064 nm), under air, at a growth rate of 15 mm/h and a relative rotation of 18 rpm between seed and feed. Using these growth conditions and adjusting the laser power input to obtain a molten zone of approximately 1–1.5 times the rod diameter, it is possible to obtain stable growth, which allows the fabrication of dimensionally homogeneous textured bars.

Bi-2212 ceramic presents incongruent melting and, in consequence, after the directional solidification process, it is necessary to perform a thermal treatment in order to produce the Bi-2212 superconducting phase. This annealing process was performed in air, and consisted of two steps: 60 h at 860 °C, followed by 12 h at 800 °C and, finally, quenched in air to room temperature.

Phase analysis of all samples was performed by powder XRD utilizing a Rigaku RadB X-ray powder diffractometer (CuKα radiation) with 2θ ranging between 5 and 65 degrees at a scan rate of 3 °/min. Microstructural and elemental analysis of the fibers, both as-grown and annealed, were studied on polished longitudinal cross-sections by using two different electron microscopes Carl Zeiss Merlin FESEM and LEO EVO-40XVP SEM equipped with Oxford instruments X-max and Bruker energy dispersive X-ray spectroscope (EDX), respectively, having a resolution up to 125 eV.

Magnetic measurements were performed in a Quantum Design PPMS (9 T). The magnetic hysteresis cycles were obtained at different temperatures (5, 15, 25 K) and the magnetic critical current density was then estimated using Bean's model. *M–T* measurements were performed when cooling the samples under applied magnetic field of 50 Oe.

3 Results and Discussion

There are two main phases appearing on polished longitudinal cross-section of as-grown rods in SEM/EDX investigations, as can be observed in Fig. 1. These are Bi rich intergrowths of 2201 and 2212 as a main matrix and Bi-free $Sr_{1-x}Ca_xCuO_2$ phase which are seen as gray and black contrasts, respectively, on the BSD images of the rods. At the highest doping level, the stoichiometry of these two phases corresponds to a cation proportion of Bi:Sr:Ca:Ni:Cu = 2,7:2:0,3:0:1,3 and 0:2:1,3:0,1:2,9, respectively, derived from EDX analysis. Especially, at the rods outer regions it can be found a higher concentration of Bi-free $Sr_{1-x}Ca_xCuO_2$ phase (black contrast) and some unreacted metallic oxides like NiO and CaO. This increase is a consequence of the incongruent melting behavior of BSCCO system which leads to the migration of Bi atoms (with the lowest melting point) from the firstly cooled border side to the inner part of the rods in the course of laser processing [16].

$Sr_{1-x}Ca_xCuO_2$ is the only phase where Ni was detected. In higher doping range, existence of Ni caused the formation of small amounts of Sr–Ni rich 2201 and 2212 intergrowths. This phase can be seen as middle gray contrast in BSD micrographs

and is indicated by arrows in Figs. 1b and 1d. As a consequence of the low doping used *(x* ≤ 0.1*)*, it could not be possible to find Ni atoms except in these two phases within the sensitivity limit of EDX detector.

For the annealed rods, the heterogeneous phase distribution seen in as-grown samples is reduced, as can be clearly seen for the $Sr_{1-x}Ca_xCuO_2$ phase (Figs. 2a–2d). Although the core of the annealed rods is mainly constituted by the Bi-2212 phase, still light gray Bi-rich 2201/2212 intergrowths persist in small amounts, indicated with white arrows in Figs. 2a–2b. Minor amounts of Sr-rich phase found in high doped as-grown rods are completely vanished upon heat treatment. At the periphery, there is still a significant amount of $Sr_{1-x}Ca_xCuO_2$ phase accompanied by some calcium oxide, probably due to the small amount of Bi in the outer region. Since the thermal annealing gives rise to more homogeneous and uniform morphology with less porosity, it is easier to notice the doping effect on the surface morphology for the annealed rods. It has been evaluated that substitution of Ni for Cu at $x = 0.1$ level introduced some local point defects to the structure which corrupts the smoothness of the surface. Upon the disappearance of Ni containing phases like $Sr_{1-x}Ca_xCuO_2$ after thermal treatment, agglomerates of nickel oxide with sizes up to a few micrometers have been started to be distinguishable on the surface, as shown in a dot mapping image in Fig. 2d. In fact, this is the desirable case from the point of view of enhanced flux pinning capability.

Figure 3 shows powder XRD patterns of pure and Ni doped annealed rods for all doping range. Since the relative amount of all secondary phases in annealed rods explained above is very small compared to the major Bi-2212 phase, the peaks originated by these phases could not be detected in the XRD spectra. It was found that for all doping range, all major peaks correspond to the Bi-2212 phase. When the doping level reached $x = 0.1$, low intensity peaks from the $n = 1$ phase (Bi-2201) were detected, suggesting that the existence of nickel in the material does not contribute to the Bi-2212 phase formation. Besides the formation of $n = 1$ phase with increasing doping level, it has also been observed a deterioration on the grains alignment, evidenced by the decrease in the relative intensity of (00l)

peaks, compared with the other (hkl) major peaks. This observation is in agreement with the SEM data discussed previously.

Transition temperature, T_c-onset, values were determined from the onset of diamagnetic signal in dc magnetization versus temperature curves between 5–130 K. Parallel to the deterioration of surface morphology and phase structure of the rods, increasing Ni substitution rate caused the degradation of T_c-onset values from about 92 to 81 K as can be observed in Fig. 4 and Table 1. Although the decrease in T_c values, transition widths from zero magnetization level to the saturation point did not show a significant change with increasing substitution rate, suggesting that Ni doping does not produce a weakening in grain connectivity within the doping range used in this work. All rods were measured in two orientations with respect to the applied field. An increase in the diamagnetic signal by a factor of ca. 7 occurred when the applied field was changed from parallel to perpendicular with respect to the growth axis.

Figure 5 shows the magnetic hysteresis (*M–H*) loops of the $x = 0.01$, $x = 0.05$ and $x = 0.1$ fibers over a temperature range of 5–25 K in fields up to 9 T. Similar to the magnetization–temperature (*M–T*) measurements, samples were placed following two different orientations with respect to the applied field. All samples showed similar symmetrical behavior which is a characteristic of HT_c superconductors. The increasing substitution rate has not caused any anomaly except a small decrease in magnetization levels of the rods. In contrast to magnetically doped Bi-2212 single crystals, peak effect has not been detected in *M–H* loops [17]. Field dependence of magnetization of the rods weakened with increasing field higher than 2 T. Critical current densities of the rods were determined from these *M–H* loops by using Bean's critical state formula which is given by [18]

$$J_{\mathrm{cmag}} = 30\frac{\Delta M}{d}$$

where ΔM is the width of the magnetization loop at applied magnetic field given by $\Delta M = M_+ - M_-$ and d is the diameter of the cylindrical sample, assuming supercurrents flow within the entire volume of the sample. As can be observed in Fig. 6, J_{cmag} *(T)* curves follow an exponential T dependence over the whole

temperature range. For the pure sample, $J_{\perp cmag}$ was found to be 5.6×10^5 A/cm^2 at 5 K and zero applied field, while for the x = 0.1 doped one in the same conditions it is reduced to 1.5×10^5 A/cm^2. At parallel applied field, these values, $J_{//cmag}$ at 5 K, were calculated to be 1.8×10^5 and 6.9×10^4 A/cm^2, respectively. Between perpendicular and parallel orientations, there is a difference by a factor ca. 3 for the undoped samples, while for the x = 0.1 doped ones this rate is around 2. This confirms that substitution of Ni caused a decrease in the anisotropy of the rods by degrading the grain orientation. When the field dependence of different doped rods is compared, it seems that there is no improvement in field dependence with increasing substitution rate. Therefore, although the agglomeration of Ni in the structure like point defects, any evidence of enhanced pinning capability in the rods with Ni substitution could not be detected from magnetic measurements.

4 Conclusions

It was found that critical current density, J_{cmag}, decreases with substitution of Ni for Cu up to x = 0.1 in $Bi_2Sr_2CaCu_{2-x}Ni_xO_{8+\delta}$. Although the existence of randomly distributed Ni agglomerates with sizes up to a few micrometers in the structure, particularly after annealing, ferromagnetic Ni impurities did not enhance magnetic coupling which eventually will cause stronger vortex interactions and higher critical current densities in the superconducting rods. Increasing substitution rate of Ni caused a depression of superconducting properties of the LFZ grown Bi-2212 rods by decreasing the grains orientation and forming minor amounts of low temperature superconducting Bi-2201 phase.

Acknowledgements

This work was supported by the Scientific and Technological Research Council of Turkey (TUBITAK) under 2214 International Doctoral Research Fellowship Program. A. Sotelo and M.A. Madre acknowledge MICINN-FEDER (Project MAT2008-00429) and DGA (Consolidated research group T12) for financial support.

References

1. Bolza, A., Metra, P., Nassi, M., Cavi, P.: IEEE Trans. Appl. Supercond. **7**, 2 (1997)

2. Elschner, S., Breuer, F., Wolf, A., Noe, M., Cowey, L., Bock, J.: IEEE Trans. Appl. Supercond. **1**, 1 (2001)

3. Nachtrab, W.T., Renaud, C.V., Wong, T., Liu, X.T., Shen, T.M., Trociewitz, U.P., Schwartz, J.: IEEE Trans. Appl. Supercond. **18**, 2 (2008)

4. Feigelson, R.S., Gazit, D., Fork, D.K., Geballe, T.H.: Science **240**, 1642 (1988)

5. de la Fuente, G., Diez, J.C., Angurel, L.A., Pena, J.I., Sotelo, A., Navarro, R.: Adv. Mater. **7**, 10 (1995)

6. Diez, J.C., Angurel, L.A., Miao, H., Fernandez, J.M., de la Fuente, G.F.: Supercond. Sci. Technol. **11**, 101 (1998)

7. Sotelo, A., Mora, M., Madre, M.A., Diez, J.C., Angurel, L.A., de la Fuente, G.F.: J. Eur. Ceram. Soc. **25**, 2947 (2005)

8. Mora, M., Sotelo, A., Amaveda, H., Madre, M.A., Diez, J.C., Capel, F., Lopez-Cepero, J.M.: J. Eur. Ceram. Soc. **27**, 3959 (2007)

9. Pu, M.H., Song, W.H., Zhao, B., Wu, X.C., Sun, Y.P., Du, J.J.: Supercond. Sci. Technol. **14**, 299 (2001)

10. Uthayakumar, S., Srinivasan, E., Jayavel, R., Subramanian, C.: Physica C **383**, 122 (2002)

11. Aksan, M.A., Yakıncı, M.E., Balcı, Y.: Supercond. Sci. Technol. **13**, 955 (2000)

12. Sotelo, A., Madre, M.A., Diez, J.C., Rasekh, Sh., Angurel, L.A., Martinez, E.: Supercond. Sci. Technol. **22**, 034012 (2009)

13. Mora, M., Angurel, L.A., Diez, J.C., Drost, R.J., Kes, P.H.: Physica C **372–376**, 1179 (2002)

14. Lennikov, V.V., Kazin, P.E., Tretyakov, Yu.D., de la Fuente, G.F.: Z. Anorg. Allg. Chem. **630**, 2337 (2004)

15. Angurel, L.A., de la Fuente, G.F., Badia, A., Larrea, A., Diez, J.C., Pena, J.I., Martinez, E., Navarro, R.: Narlikar, A.V. (ed.): Studies of High Temperature Superconductors, vol. 21 p. 1 Nova Science Publishers, New York (1997)

16. Natividad, E., Diez, J.C., Angurel, L.A., Andres, J.M., Ferrando, A.C., Mayoral, M.C.: Physica C **383**, 379 (2003)
17. Wang, X.L., Liu, H.K., Dou, S.X., Horvat, J., Gu, G.D.: Supercond. Sci. Technol. **15**, 356 (2002)
18. Bean, C.P.: Phys. Rev. Lett. **8**, 250 (1962)

Table 1. T_c-onset values of the annealed rods obtained by the *M*–*T* plots in Fig. 4

	$T^{\perp}_{\text{c-onset}}$ (K)	$T^{//}_{\text{c-onset}}$ (K)
Pure	92.1	91.9
$X = 0.01$	89.9	89.7
$X = 0.03$	86.4	86
$X = 0.05$	83	82.7
$X = 0.1$	81	81

Figure captions

Figure 1. BSD images and dot mapping analysis obtained on inner parts of longitudinal polished sections of as-grown rods: (**a**) x = 0.01, (**b**) x = 0.05, (**c**) x = 0.03, (**d**, **e**, **f**) x = 0.1. The representative colors for each element are: Bi: *red*, Sr: *green*, Ca: *blue*, Cu: *light blue*, Ni: *pink arrows* in higher doped ones indicate the low amount of Sr–Ni rich 2201/2212 intergrowths formed after Ni substitution at the level of $x \geq 0.05$. This phase disappeared after heat treatment

Figure 2. BSD images and dot mapping analysis obtained on inner parts of longitudinal polished sections of annealed rods: (**a**) x = 0.01, (**b**) x = 0.05, (**c**, **d**) x = 0.1. The representative colors for each element are: Bi: *red*, Sr: *green*, Ca: blue, Cu: *light blue*, Ni: *pink*. *Black arrows* in (**a**–**b**) indicate the Bi-rich 2201/2212 intergrowths having same stoichiometry with the main phase of as-grown rods. *White arrows* show the agglomeration of Ni that took place after heat treatment

Figure 3. Powder XRD patterns of pure and Ni-doped annealed textured rods. Increasing doping rate caused the appearance of minor amount of secondary poor superconducting phase, 2201

Figure 4. Temperature dependence of magnetization of the annealed rods at fields applied both parallel and perpendicular to the growth axis. Measurements were performed on samples cooled under applied field

Figure 5. Magnetization vs. magnetic field curves of Ni-doped annealed rods at 5, 15, and 25 K

Figure 6. Semi-logarithmic plots of calculated magnetic critical current densities of the annealed rods at all doping range between 0–9 T and at 5, 15, 25 K temperatures

Figure 1

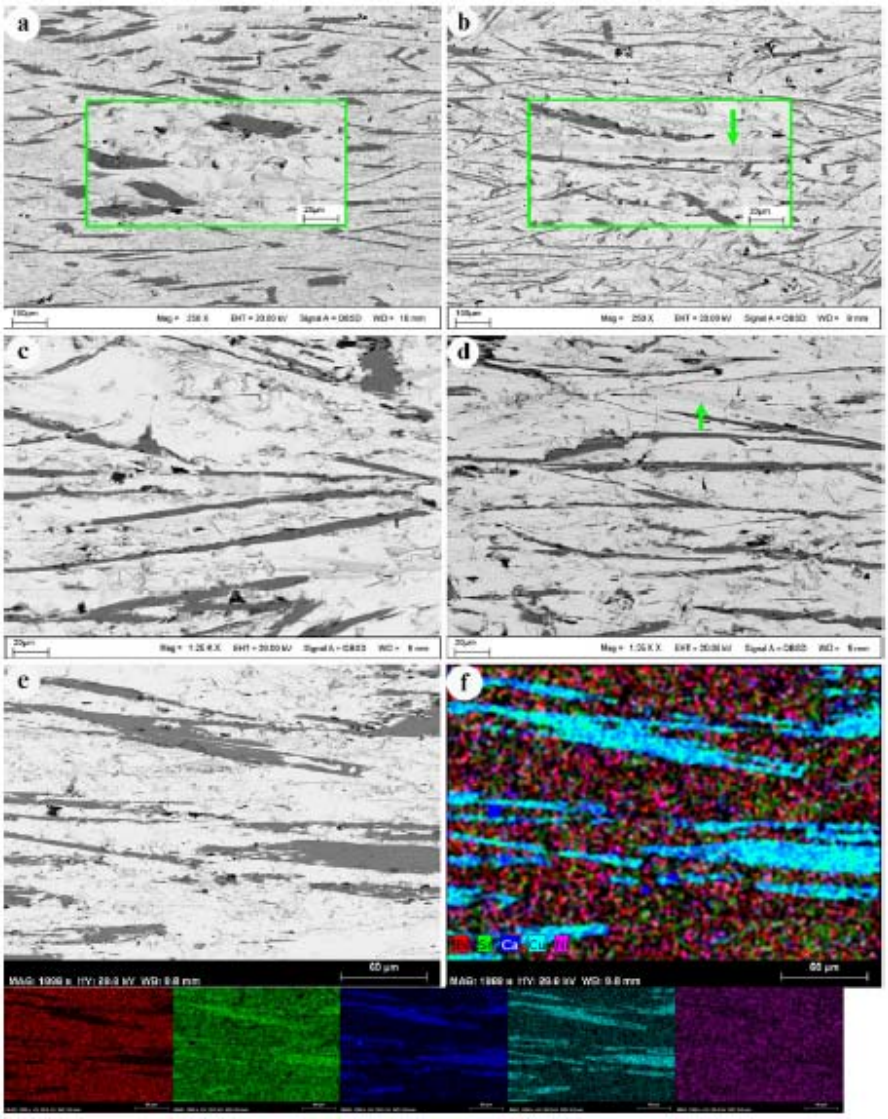

Figure 2

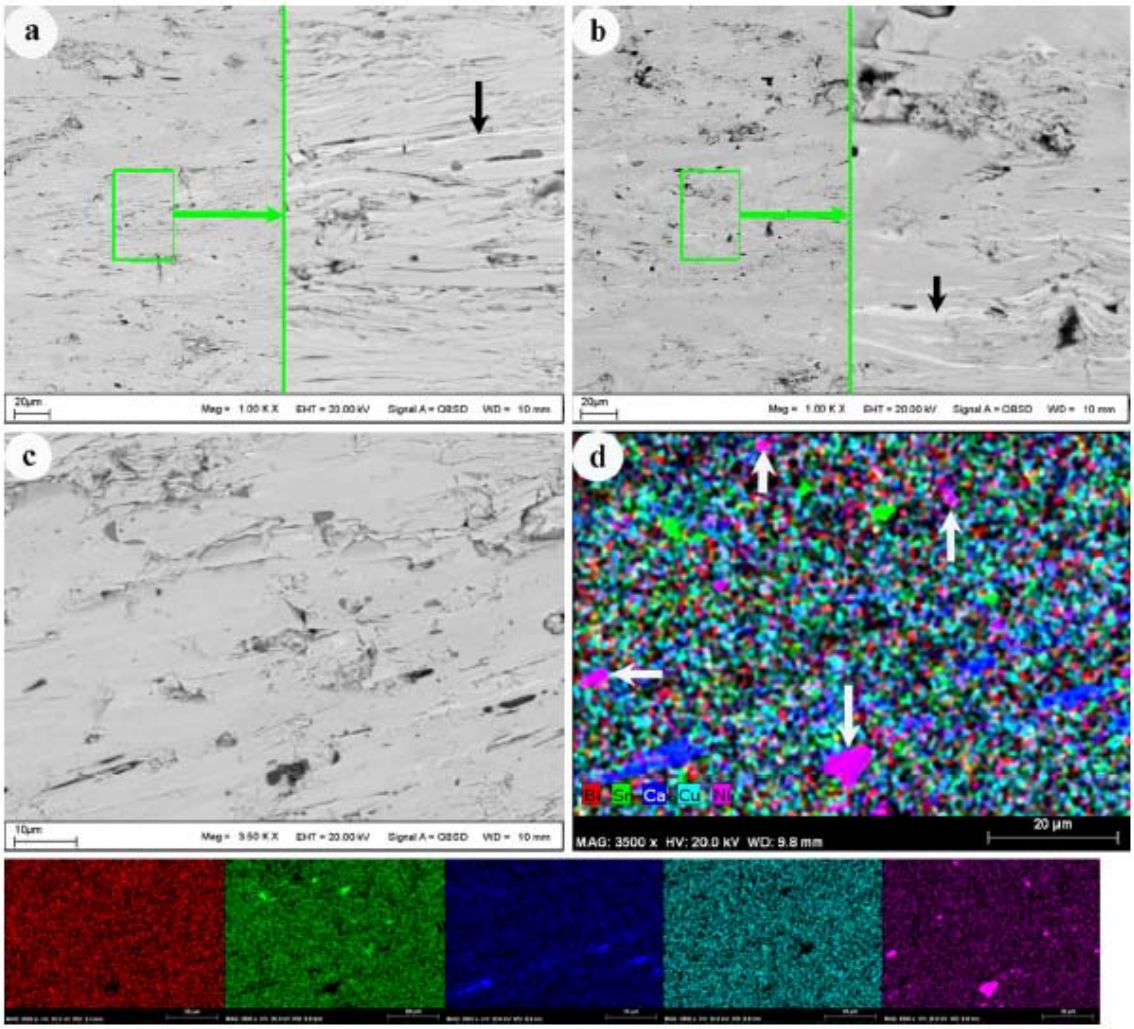
a
b
c
d
20μm
Mag = 1.00 K X EHT = 20.00 kV Signal A = QBSD WD = 10 mm
10μm
Mag = 3.50 K X EHT = 20.00 kV Signal A = QBSD WD = 10 mm
Sn
Ce
Cu
Ni
MAG: 3500 x HV: 20.0 kV WD: 9.8 mm
20 μm

Figure 3

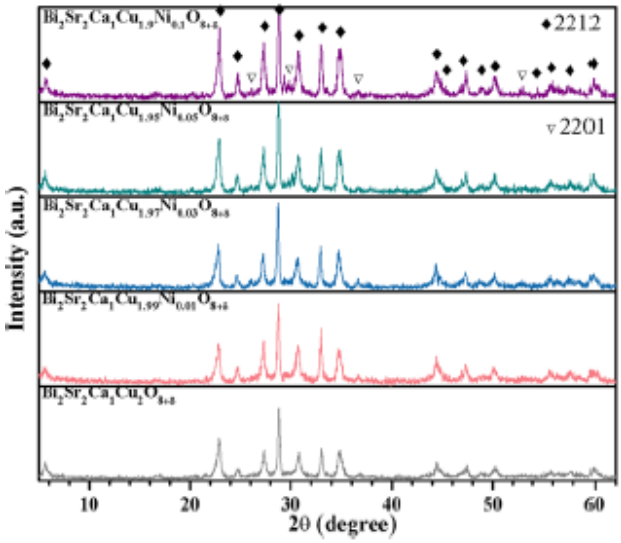
Bi2Sr2Ca1Cu1.9Ni0.1O8+δ
Bi2Sr2Ca1Cu1.95Ni0.05O8+δ
Bi2Sr2Ca1Cu1.97Ni0.03O8+δ
Bi2Sr2Ca1Cu1.99Ni0.01O8+δ
Bi2Sr2Ca1Cu2O8+δ
♦2212
▽2201
Intensity (a.u.)
10
20
30
40
50
60
2θ (degree)

Figure 4

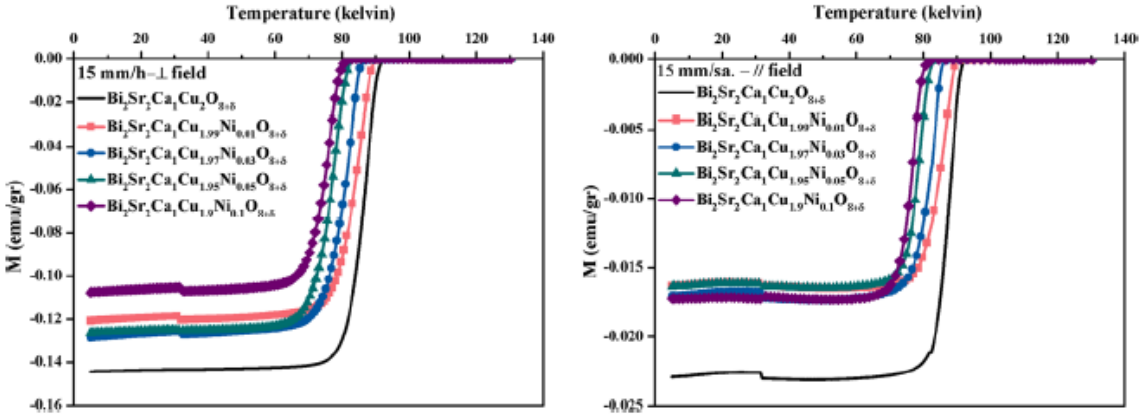
Temperature (kelvin)
M (emu/gr)
15 mm/h–⊥ field
Bi2Sr2Ca1Cu2O8+δ
Bi2Sr2Ca1Cu1.99Ni0.01O8+δ
Bi2Sr2Ca1Cu1.97Ni0.03O8+δ
Bi2Sr2Ca1Cu1.95Ni0.05O8+δ
Bi2Sr2Ca1Cu1.9Ni0.1O8+δ
Temperature (kelvin)
M (emu/gr)
15 mm/sa. – // field
Bi2Sr2Ca1Cu2O8+δ
Bi2Sr2Ca1Cu1.99Ni0.01O8+δ
Bi2Sr2Ca1Cu1.97Ni0.03O8+δ
Bi2Sr2Ca1Cu1.95Ni0.05O8+δ
Bi2Sr2Ca1Cu1.9Ni0.1O8+δ

Figure 5

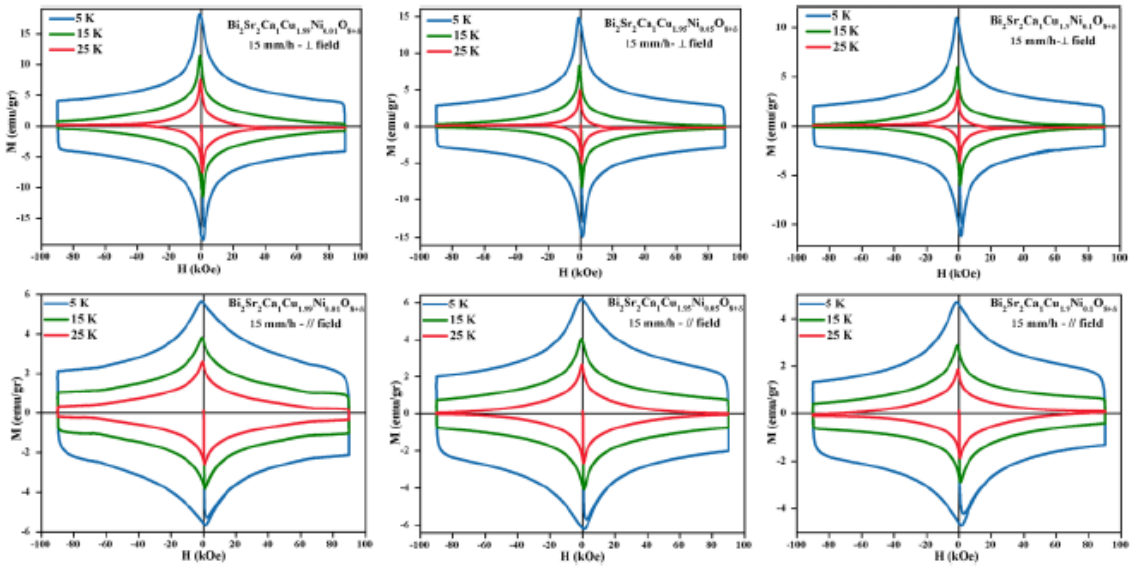

Figure 6

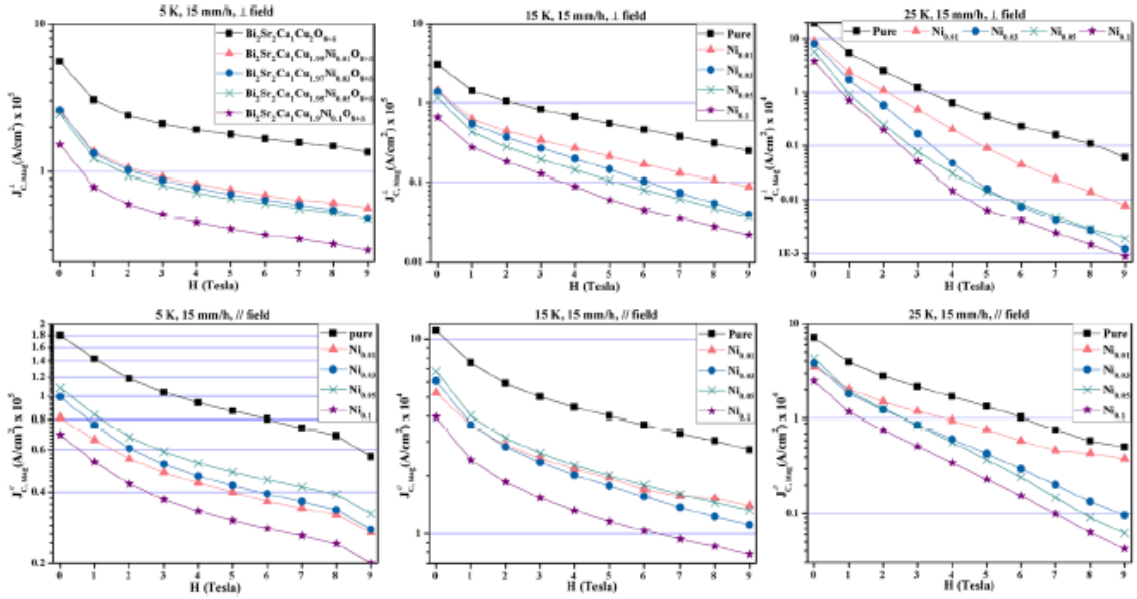
5 K, 15 mm/h, ⊥ field
15 K, 15 mm/h, ⊥ field
25 K, 15 mm/h, ⊥ field
5 K, 15 mm/h, // field
15 K, 15 mm/h, // field
25 K, 15 mm/h, // field
Pure
H (Tesla)